

The lithology and composition of lunar mantle modified by ilmenite bearing cumulate: A thermodynamic model

Wei Huang^{1,2} · Wei Du^{1,3} 

Received: 14 May 2024 / Revised: 18 June 2024 / Accepted: 25 June 2024 / Published online: 12 July 2024

© The Author(s), under exclusive licence to Science Press and Institute of Geochemistry, CAS and Springer-Verlag GmbH Germany, part of Springer Nature 2024

Abstract Due to their high density, the ilmenite-bearing cumulates (IBC) (with or without KREEP) formed during the late-stage lunar magma ocean solidification are thought to sink into the underlying lunar mantle and trigger lunar mantle overturn. Geophysical evidence implied that IBC may descend deep inside the Moon and remain as a partially molten layer at the core-mantle boundary (CMB). However, partial melting may have occurred on the mixed mantle cumulates during the sinking of IBC/KREEP and the silicate melt may be positively buoyant, thus preventing the IBC/KREEP layer from sinking to the CMB. Here, we perform thermodynamic simulation on the stability of lunar mantle cumulates at different depths mixed with different amounts of IBC/KREEP from an updated LMO model. The modeling results suggest that the sinking of IBC/KREEP will cause at least 5 wt% partial melting in the shallow (~120 km) and a much larger degree of partial melting in the deep lunar mantle (~420 km). Due to the density contrast with the surrounding mantle, IBC/KREEP-bearing melts could potentially decouple under certain conditions. The modified lunar mantle by sinking of IBC/KREEP can better explain the formation of different kinds of lunar basaltic magma than the

primary lunar mantle formed through differentiation of lunar magma ocean. Sinking of IBC/KREEP back into the lunar mantle may introduce plagioclase, clinopyroxene, garnet, and incompatible radioactive elements into the deep lunar mantle, which will further affect the thermal and chemical evolution of the lunar interior.

Keywords Ilmenite-bearing cumulate · KREEP · Partial melting · Lunar mantle overturn · pMELTS

1 Introduction

The Moon is hypothesized to have originated from a debris disk formed by a giant impact between the proto-Earth and a Mars-sized impactor, Theia. The subsequent accretion process is believed to have generated sufficient heat to produce a large-scale, potentially even Moon-wide magma ocean (Lunar Magma Ocean, LMO) (e.g., Canup and Asphaug 2001; Ćuk and Stewart 2012; Hartmann and Davis 1975). Many different models have been proposed to describe the differentiation process of LMO (e.g., Charlier et al. 2018; Elkins-Tanton et al. 2011; 2017; Lin et al. 2020; Rapp and Draper 2018; Schmidt and Kraettli 2022; Snyder et al. 1992). These LMO solidification models suggest that Mg-rich minerals crystallized first from the cooling LMO to form the primitive mantle, followed by plagioclase crystallizing and rising to form the anorthositic crust. Ilmenite-bearing cumulates (IBC) and urKREEP (LMO residuum enriched in potassium, rare earth elements, and phosphorus) formed at the final stage of the LMO solidification are thought to have a significant effect on the thermo-chemical evolution of the lunar interior (Hess and Parmentier 1995; Zhao et al. 2019; Zhong et al. 2000). Due to their high density, the IBC layer, with or without the KREEP component, is gravitationally

Supplementary Information The online version contains supplementary material available at <https://doi.org/10.1007/s11631-024-00718-x>.

✉ Wei Du
duwei@mail.gyig.ac.cn

¹ State Key Laboratory of Ore Deposit Geochemistry, Institute of Geochemistry, Chinese Academy of Sciences, Guiyang 550081, China

² University of Chinese Academy of Sciences, Beijing 100049, China

³ Center for Excellence in Comparative Planetology, Chinese Academy of Sciences, Hefei 230026, China

unstable and susceptible to Rayleigh–Taylor instabilities. This instability can trigger the foundering of the IBC layer into the underlying lunar mantle cumulate, potentially initiating lunar mantle overturn (Elkins Tanton et al. 2002; Hess and Parmentier 1995).

Lunar mantle overturn may have induced potential partial melting within the lunar mantle, primarily through two mechanisms: (1) the introduction of LMO late-stage, low-melting temperature components lowered the solidus temperature of the deep mantle, causing partial melting, or (2) the ascent of deep mafic material resulted in adiabatic decompression melting. These processes generated relatively ancient cryptomare basalt, mg-suite, and other products of early lunar magmatic activity (Elardo et al. 2011; Prissel and Gross 2020; Shearer et al. 2015; Zhong et al. 2000). Geophysicists have proposed that there is a boundary layer containing melt at the core–mantle boundary of the Moon (Garcia et al. 2011; Khan et al. 2004, 2014; Weber et al. 2011), and the formation of this melted layer may also be related to IBC (Parmentier et al. 2002; van Kan Parker et al. 2012; Zhang et al. 2017; Zhong et al. 2000). In other words, the IBC layer can sink deep into the core–mantle boundary of the Moon.

Nonetheless, the lunar mantle overturn scenario as the driving mechanism for early lunar magmatic activities has been criticized and the initiation and duration of lunar mantle overturn remain controversial. According to the LMO model, plagioclase crystallization (forming the primary anorthositic lunar crust) occurred near the end of LMO differentiation (> 70 PCS), while ilmenite crystallization began later than plagioclase, during ~ 88–97 PCS (Charlier et al. 2018; Elardo et al. 2011; Ju et al. 2022; Lin et al. 2017; Snyder et al. 1992). If the formation of intrusive Mg-suite and alkali-suite within the lunar crust resulted from an IBC-induced mantle overturn, they should be formed after the lunar crust's formation. However, the available age data for lunar samples indicate a heavy overlap among the early lunar magmatic samples (e.g., Borg et al. 2011, 2020). To explain the overlapping age, some researchers proposed that the lunar mantle overturn caused by sinking of IBC occurred before the end of LMO differentiation, that is, the formation of the lunar crust was accompanied by the lunar mantle overturn (Borg et al. 2015; Boukaré et al. 2018; Elardo et al. 2011; Maurice et al. 2017; Prissel and Gross 2020; Shearer et al. 2015). To some extent, the formation of IBC is instantaneous with the crystallization of some plagioclase, thus the initiation of IBC sinking can occur at a relatively early stage. However, the question remains. The melting temperature of IBC is relatively low (< 1000 °C) (e.g., Ju et al. 2022) and the temperature inside the Moon at the early stage could be much higher than 1000 °C, thus re-entry of these dense and low-melting materials into the lunar

mantle will inevitably lead to partial melting of the lunar mantle cumulates. Therefore, whether IBC can successfully reach the lower lunar mantle, remains to be verified by experiments or theoretical studies.

Previous studies have emphasized the importance of IBC in the early lunar magmatic activity (Hess and Parmentier 1995; 2001), and the rheological properties of ilmenite-bearing cumulates have also been studied by high-temperature and high-pressure experiments (Dygert et al. 2016, 2017; Pommier et al. 2024). These new physical properties data about IBC set new parameters for the dynamic simulation of the lunar mantle overturn process, providing new constraints on simulating the “fate” of IBC. However, most dynamic simulations assume that the subsidence process is mainly solid flow, and the occurrence of Rayleigh instability is largely dependent on the relative viscosity of the IBC layer and the surrounding rock (e.g., Elkins Tanton et al. 2002; Hess and Parmentier 1995). Therefore, the subsidence mode and extent of IBC are not only affected by the thickness of the IBC layer but also depend on the composition and the thermal state of the lunar mantle at the time of the overturn (e.g., Li et al. 2019; Zhang et al. 2022; Zhao et al. 2019). Such information is mainly dependent on the interpretation of the few available lunar earthquake data and experimental constraints (Garcia et al. 2011, 2019; Harada et al. 2014; Khan et al. 2014; Matsumoto et al. 2015). Most importantly, the available dynamic simulations do not consider the reaction between IBC or KREEP with the lunar mantle cumulates during the sinking process (e.g., Li et al. 2019). Moreover, the LMO model has been updated in many aspects, such as the depth of the lunar magma ocean, the mineral composition and structure of the deep Moon, and the time and thickness of the crystallization of the IBC layer (Jing et al. 2022; Johnson et al. 2021; Lin et al. 2017, 2020; Rapp and Draper 2018).

As mentioned above, if IBC occurs in partial melting during subsidence or induces partial melting of deep lunar mantle cumulates, it will inevitably change the properties of the IBC layer, including chemical composition, viscosity, density, etc. The extraction of the formed melt (mostly titanium-rich melt) (whether floating or sinking) should leave a considerable change on the primitive lunar mantle. In this study, we adopt new parameters from the updated LMO models and perform thermodynamic calculations by using the algorithm pMELTS to investigate the fate of the IBC/KREEP layer in the lunar mantle. We constrain the partial melting conditions of the mixed lunar mantle cumulates at different depths and the composition and migration of the melting products; we also explore whether the IBC and KREEP are decoupled during lunar mantle overturn, and the composition and structure of the lunar mantle modified by lunar mantle overturn process.

2 Methods

2.1 Composition of IBC and lunar mantle cumulates

There have been several high-temperature and high-pressure experimental studies and numerical simulations on LMO models (Charlier et al. 2018; Elkins-Tanton et al. 2011; 2017; Lin et al. 2020; Rapp and Draper 2018; Schmidt and Kraettli 2022; Snyder et al. 1992). Although these models adopted different initial bulk compositions and depth of LMO and different crystallization modes, these LMO models generally agree that a variety of mafic lithologies (olivine, orthopyroxene, and clinopyroxene) were produced at the early stage of the LMO fractionation and formed a heterogeneous mantle. In this study, we chose mantle cumulates and IBC/KREEP from the LMO model by Lin et al. (2017), which sets LMO depth as ~700 km (3 GPa) contrasting with earlier shallow LMO models that typically assumed a depth of 400 km (Snyder et al. 1992). This two-stage (refers to the LMO solidification that transitions from an initial equilibrium crystallization stage to subsequent fractional crystallization process) LMO model formed a stratigraphic layered lunar interior from top to bottom as anorthosite crust (plagioclase + quartz), followed by the IBC layer (ilmenite + clinopyroxene) and the upper lunar mantle as olivine + clinopyroxene layer, and the lower lunar mantle as olivine + orthopyroxene cumulates. It offers a more complete mineralogical composition and elemental abundances of both the upper and lower lunar mantle, as well as the IBC and KREEP components. In contrast, other LMO models are not taken as examples due to either a shallow magma ocean (Snyder et al. 1992) or continuous fractional crystallization throughout the entire process (Rapp and Draper 2018; Schmidt and Kraettli 2022). To simplify the model, we merged several small layers with nearly identical compositions and divided the LMO primitive cumulates into three distinct lunar stratigraphies: the lower lunar mantle (75% olivine + 25% orthopyroxene), the upper lunar mantle (11% olivine + 89% clinopyroxene), and the IBC layer (85% clinopyroxene + 15% ilmenite) (Table 3). It should be noted that in most LMO models, the lowermost cumulate layer is dunite (e.g., Charlier et al. 2018; Elardo et al. 2011; Ju et al. 2022; Snyder et al. 1992), while the lower lunar mantle cumulates used in this study is a harzburgite layer, which may lead to a relatively lower melting temperature of this layer.

2.2 Thermodynamic calculation

Different degrees of partial melting on the mixed cumulates in the lunar mantle following the lunar mantle overturn has been simulated using the thermodynamic phase-equilibrium program pMELTS_v5.6.1 (Ghiorso et al. 2002). It is

an updated version of the MELTS program (Ghiorso and Sack 1995) that simulates the solid–solid and solid–liquid phase equilibrium in silicate systems at high-temperature and high-pressure conditions. pMELTS is applicable to the pressure ranges of 1–3 GPa and is widely used to simulate various igneous processes on the Moon (Arai and Maruyama 2017; Elardo and Astudillo Manosalva 2023; Klaver et al. 2024, 2021; Luo et al. 2023). To simulate the possible mixed lunar mantle compositions after lunar mantle overturn, different amounts (0 wt%, 10 wt%, 20 wt%, 30 wt%, 40 wt% and 50 wt%) of the late components from LMO model (IBC and KREEP, compositions are shown in Tables 1 and 2, compared with compositions reported in other studies) (Ju et al. 2022; Lin et al. 2017; Neal and Taylor 1989; Van Orman and Grove 2000; Warren 1989) were added to olivine + clinopyroxene layer at 0.6 GPa (the shallow lunar mantle) and olivine + orthopyroxene layer at 2 GPa (the deep lunar mantle), respectively (Table 3). We then performed phase equilibrium calculations on the possible melting process resulting from these mixed mantle components to obtain melting temperatures at different degrees of partial melting (5 wt%, 10 wt%, 20 wt%, 30 wt%, 40 wt% and 50 wt%). The oxygen fugacity in the calculations was controlled at the iron-wüstite (IW) buffer, which is considered to closely approximate the oxygen fugacity conditions within the lunar interior (Elardo and Astudillo Manosalva 2023; Longhi 1992; Luo et al. 2023). In the calculation process, we can track the composition and density of the melt and the mineral assemblage of the residual solid. In pMELTS, the density of melt is calculated using a third-order Birch-Murnaghan equation of state (Ghiorso et al. 2002):

Table 1 Compositions of IBCs from different LMO models

wt%	Lin et al. (2017) ^a	Ju et al. (2022) ^b	TiCum ^c
SiO ₂	45.20	45.52	41.61
TiO ₂	9.22	1.65	9.10
Al ₂ O ₃	2.56	1.74	2.80
Cr ₂ O ₃	–	1.37	0.00
FeO	23.91	22.72	29.60
MnO	–	0.42	0.00
MgO	16.84	11.90	7.50
CaO	3.08	14.64	8.20
Na ₂ O	–	0.03	0.00
K ₂ O	–	0.00	0.00
Mg#	55.66	48.29	31.11

^aIntegration of two ilmenite-rich layers

^bIntegration of the last four layers within the 1000 km LPUM-LMO in the Ju et al. (2022) model

^cComposition from Van Orman and Grove (2000), which is similar to the solid assemblage proposed by Snyder et al. (1992) after 95 PCS

Table 2 Compositions of KREEP from different LMO models and petrological studies

	wt%	Lin et al. (2017) ^a	Ju et al. (2022) ^b	Rapp and Draper (2018)	High-K KREEP ^c	urKREEP ^d
SiO ₂	46.26	42.71	39.61	50.28	45.60	
TiO ₂	5.14	3.91	3.51	2.00	2.62	
Al ₂ O ₃	8.78	7.16	5.91	15.12	7.59	
Cr ₂ O ₃	—	0.06	—	0.18	0.00	
FeO	26.45	29.43	32.75	10.29	27.80	
MnO	—	0.65	0.66	0.14	0.00	
MgO	2.01	0.41	0.89	8.29	0.42	
CaO	11.01	14.91	11.32	9.79	9.42	
Na ₂ O	—	0.30	0.52	0.94	0.22	
K ₂ O	—	0.30	0.24	0.96	1.29	
P ₂ O ₅	—	—	4.20	0.80	3.85	
Mg#	11.93	2.42	4.62	58.95	2.62	

^aComposition from the melt at 96.4–99.9 PCS^bComposition from the melt at 97.8–99.6 PCS of 1000 km LPUM-LMO^cComposition from Warren (1989)^dComposition from Neal and Taylor (1989)**Table 3** Compositions of lunar mantle cumulates from different LMO models

	Lin et al. (2017)	Lin et al. (2017)	Ju et al. (2022)	Ju et al. (2022)	Elardo et al. (2011)	Elardo et al. (2011)
	0.6 GPa	2 GPa	0.53 GPa	1.89 GPa	1 GPa	2 GPa
SiO ₂	51.57	43.80	45.68	52.48	45.58	44.65
TiO ₂	0.67	0.06	0.08	0.02	0.03	0.01
Al ₂ O ₃	3.78	0.70	1.71	1.16	1.04	0.80
Cr ₂ O ₃	—	—	0.95	0.36	0.55	0.46
FeO	13.51	9.07	16.57	4.66	7.20	7.14
MnO	—	—	0.25	0.08	0.10	0.10
MgO	27.50	45.94	33.30	40.72	45.59	45.73
CaO	2.93	0.40	1.43	0.53	0.77	0.39
Na ₂ O	—	—	0.02	0.01	0.00	0.00
K ₂ O	—	—	0.00	0.00	0.00	0.00
Mg#	78.40	90.03	78.17	93.97	91.86	91.94

The LMO cumulate compositions of Lin et al. (2017) and Ju et al. (2022) have been merged and simplified appropriately, and the compositions of Elardo et al. (2011) cumulate are all derived from LPUM-LMO

$$P = \frac{3}{2}K \left[\left(\frac{V_0}{V} \right)^{\frac{7}{3}} - \left(\frac{V_0}{V} \right)^{\frac{5}{3}} \right] \left\{ 1 - \frac{3}{4}(4 - K') \left[\left(\frac{V_0}{V} \right)^{\frac{2}{3}} - 1 \right] \right\} \quad (1)$$

In this equation, the reference volume (V_0), isothermal bulk modulus (K), and the pressure derivative of the bulk modulus (K') are all calibrated using experimental data (e.g., Agee and Walker 1993; Miller et al. 1991). Notably, pMELTS demonstrates a good prediction with the density of Apollo 14 black glass at its liquidus temperature (Carcione and Agee 1996; Ghiorso et al. 2002), suggesting that pMELTS provides a reasonable estimate of the density of high-Ti lunar magmas.

3 Results

3.1 The effect of IBC/KREEP on the melting temperature of lunar mantle cumulates at different depth

Figure 1 shows the effect of IBC and KREEP on melting temperature of lunar mantle cumulates in the shallow (0.6 GPa, ~120 km, Tables 4 and 6) and deep (2 GPa, ~420 km, Tables 5 and 7) lunar mantle. Hybridizing the primitive lunar mantle cumulates crystallized from LMO with IBC/KREEP can dramatically lower the melting temperature of the mantle mixtures. To generate 5 wt%

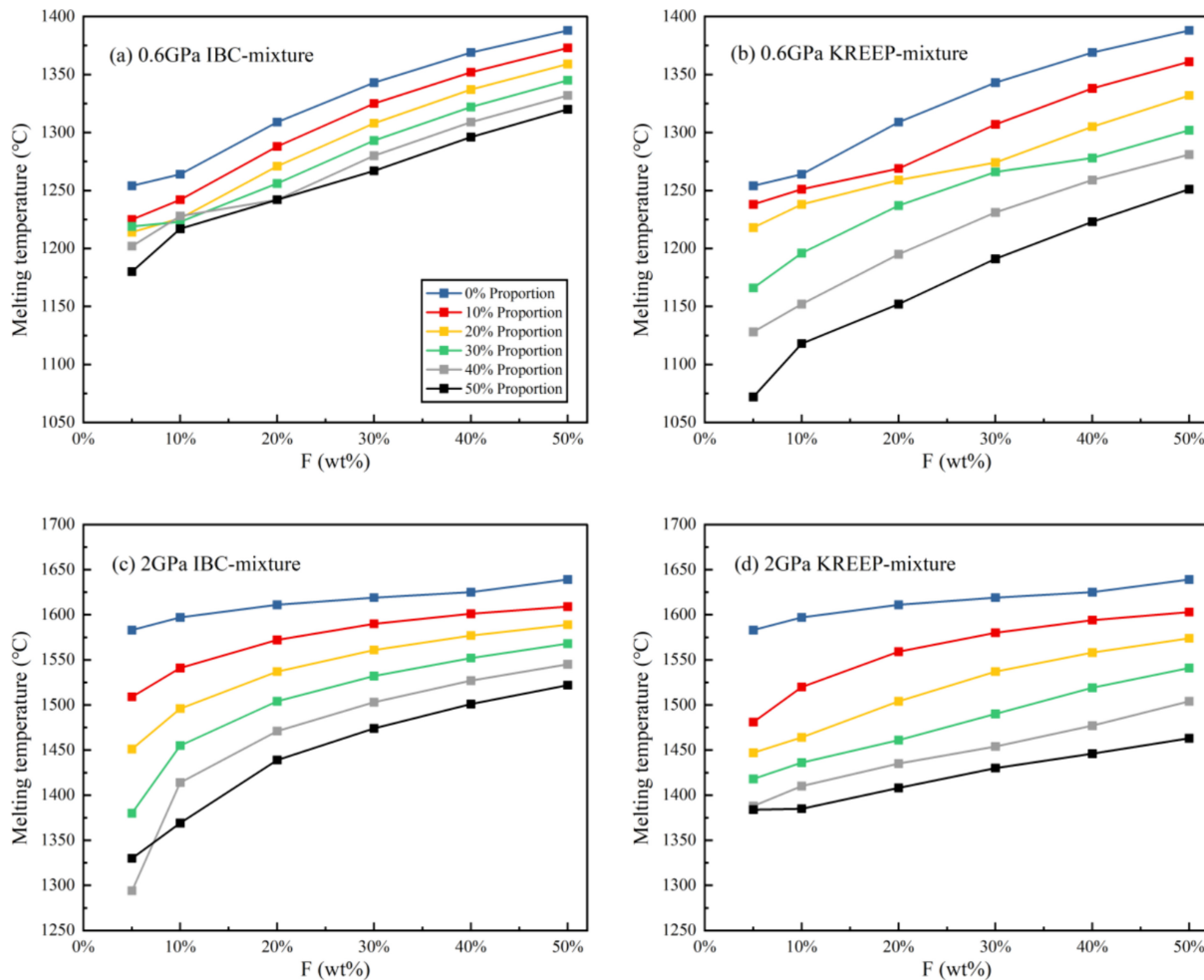


Fig. 1 Melting temperatures of IBC/KREEP mixed with lunar mantle cumulates under two different pressure conditions calculated by pMELTS. The melting temperatures of **a** IBC mixture at 0.6 GPa; **b** KREEP mixture at 0.6 GPa; **c** IBC mixture at 2 GPa; **d** KREEP mixture at 2 GPa

of melt in the upper lunar mantle, the addition of 10 wt% IBC can lower the melting temperature by ~ 30 °C and if the fraction of IBC is as large as 50 wt%, the melting temperature can drop to 1180 °C, which is about ~ 70 °C lower than the melting temperature of the primitive lunar mantle cumulates formed through lunar magma ocean differentiation (Ju et al. 2022). The melting temperatures of the deeper lunar mantle (2 GPa) appeared to be more sensitive to the mixing with these late LMO components, especially for the relatively small amount of addition of IBC (< 30 wt%) (Fig. 1c). For the lower lunar mantle, the addition of 10 wt% IBC can lower the melting temperature by 74 °C when the partial melting degree is about 5 wt% and the melting temperature drops to 1330 °C when the amount of IBC is 50 wt%, which is about 250 °C lower than the melting temperature of the primitive lower lunar mantle. The overall effect of KREEP material on lowering the melting temperature (Fig. 1b, d) is more profound than that of IBC (Fig. 1a, c), showing that an

increase in the proportion of KREEP leads to a faster decrease in the melting temperature compared to adding IBC. For the upper lunar mantle, to get a relatively lower degree of melting (< 10 wt%), adding IBC and KREEP shows a similar effect on the melting temperature of the mixture when the fraction of IBC/KREEP is no more than 20% (Fig. 1a, b). Considering a partial melting degree of 5 wt%, when the amount of IBC/KREEP increases from 30 wt% to 50 wt%, mixing with KREEP material can dramatically lower the melting temperature (ΔT is ~ 100 °C) while adding 20 wt% more IBC only lower the melting temperature from 1219 to 1180 °C (Table S3, Table 6). However in the case of a larger degree of partial melting ($F \geq 30$), the KREEP curve is still below that of IBC (Fig. 1a, b). The difference between the two curves is smaller at higher pressure compared to the low pressure, meaning that in the lower lunar mantle, the difference of influence on melting temperature between IBC-bearing and KREEP-bearing mantle cumulates becomes smaller

Table 4 pMELTS calculation results of melts compositions (wt%) for the Lin et al. (2017) mantle cumulate at ~ 120 km (0.6 GPa) within the lunar mantle with varying IBC fractions and degrees of partial melting

Melt Frac.	IBC Frac.	SiO ₂	TiO ₂	Al ₂ O ₃	Cr ₂ O ₃	FeO	MnO	MgO	CaO	Na ₂ O	K ₂ O	mg#
F=5	0%	43.61	5.61	13.99	—	15.88	—	9.41	11.10	—	—	51.37
	10%	34.64	19.08	11.36	—	15.84	—	7.30	11.35	—	—	45.11
	20%	30.07	27.55	9.71	—	15.18	—	6.10	10.97	—	—	41.72
	30%	31.01	25.98	9.27	—	16.23	—	6.29	10.78	—	—	40.88
	40%	26.86	36.02	7.79	—	14.08	—	4.65	10.21	—	—	37.04
	50%	23.38	44.65	6.74	—	12.24	—	3.39	9.26	—	—	33.08
	F=10	0%	44.88	4.29	13.70	—	15.92	—	9.70	11.09	—	—
F=20	10%	39.44	11.59	11.99	—	16.94	—	8.51	11.09	—	—	47.23
	20%	34.19	19.89	10.44	—	17.08	—	7.15	10.80	—	—	42.72
	30%	32.53	22.96	9.50	—	17.38	—	6.68	10.49	—	—	40.65
	40%	33.46	21.47	8.97	—	18.55	—	6.89	10.19	—	—	39.84
	50%	30.79	28.31	7.92	—	17.26	—	5.52	9.76	—	—	36.33
	0%	47.60	2.81	11.69	—	16.77	—	12.29	8.44	—	—	56.65
	10%	44.10	6.74	10.74	—	18.16	—	11.26	8.57	—	—	52.50
F=30	20%	40.83	10.83	9.88	—	19.23	—	10.18	8.60	—	—	48.54
	30%	37.75	15.05	9.12	—	19.99	—	9.02	8.61	—	—	44.58
	40%	34.84	19.39	8.41	—	20.43	—	7.83	8.61	—	—	40.59
	50%	34.90	19.34	7.87	—	21.15	—	7.69	8.55	—	—	39.34
	0%	49.58	2.07	9.77	—	16.86	—	14.57	6.74	—	—	60.64
	10%	46.93	4.76	9.11	—	18.33	—	13.70	6.74	—	—	57.12
	20%	44.34	7.55	8.54	—	19.65	—	12.69	6.78	—	—	53.52
F=40	30%	41.90	10.37	8.01	—	20.80	—	11.65	6.79	—	—	49.96
	40%	39.68	13.14	7.48	—	21.81	—	10.64	6.77	—	—	46.51
	50%	37.50	16.04	7.01	—	22.63	—	9.54	6.78	—	—	42.91
	0%	51.20	1.61	8.16	—	16.45	—	16.56	5.64	—	—	64.21
	10%	48.94	3.68	7.73	—	17.91	—	15.67	5.65	—	—	60.94
	20%	46.82	5.75	7.29	—	19.28	—	14.80	5.63	—	—	57.77
	30%	44.70	7.89	6.92	—	20.59	—	13.79	5.65	—	—	54.42
F=50	40%	42.78	9.96	6.52	—	21.79	—	12.84	5.63	—	—	51.23
	50%	40.89	12.11	6.16	—	22.90	—	11.81	5.64	—	—	47.89
	0%	52.51	1.31	6.94	—	15.76	—	18.19	4.90	—	—	67.29
	10%	50.56	2.98	6.62	—	17.17	—	17.37	4.90	—	—	64.32
	20%	48.68	4.65	6.30	—	18.54	—	16.52	4.88	—	—	61.37
	30%	46.81	6.37	6.01	—	19.89	—	15.59	4.89	—	—	58.27
	40%	45.04	8.06	5.71	—	21.18	—	14.65	4.89	—	—	55.21
	50%	43.39	9.72	5.40	—	22.40	—	13.73	4.87	—	—	52.21

(Fig. 1c, d). In the case of F=50, the fractions of IBC/KREEP are 30 wt%, 40 wt%, and 50 wt%, and the melting temperature differences of the two different mixed cumulates in the shallow part of the lunar mantle are 43 °C, 51 °C and 69 °C, respectively, while in the deeper lunar mantle, the difference is relatively smaller as 27 °C, 41 °C and 59 °C, respectively.

For the deeper lunar mantle, the small amount of IBC/KREEP shows huge impact on the melting temperature of the mixed cumulates, but the effect of IBC/KREEP becomes less evident as the amount of IBC/KREEP in the mixture increases (Fig. 1c, d). For example, for 5 wt% partial melting, the addition of the first 10 wt% KREEP causes

the melting temperature of the lunar mantle cumulates to decrease by 102 °C, while the effect of 50 wt% KREEP on melting temperature is only 4 °C lower than that of 40 wt% of KREEP on the lower lunar mantle cumulates. It is worth noting that to make small degree of partial melting of the lower lunar mantle cumulate, the effect on melting temperature of KREEP is less profound than that of IBC when the addition of late LMO components is more than 20 wt% (Fig. 1c, d), and the addition of 10 wt% more IBC (from 40 wt% to 50 wt%) to the lower lunar mantle causes the melting temperature increased (Fig. 1c). A similar situation occurred in the case of KREEP as well although not as

Table 5 Thermodynamic calculation results of melts compositions (wt%) for the Lin et al. (2017) mantle cumulate at ~ 420 km (2 GPa) within the lunar mantle with varying IBC fractions and degrees of partial melting

Melt Frac.	IBC Frac.	SiO ₂	TiO ₂	Al ₂ O ₃	Cr ₂ O ₃	FeO	MnO	MgO	CaO	Na ₂ O	K ₂ O	mg#
F=5	0%	43.36	0.80	6.00		16.27		31.11	2.21			77.31
	10%	34.99	15.52	4.02		16.85		23.71	4.65			71.49
	20%	27.70	31.47	2.97		15.09		15.87	6.66			65.21
	30%	20.94	48.08	2.12		11.87		9.21	7.58			58.03
	40%	14.57	63.87	1.30		8.74		5.10	6.27			50.98
	50%	18.59	53.46	1.59		12.21		6.38	7.56			48.23
	F=10	0%	44.56	0.49	4.41	15.79		32.87	1.64			78.77
F=20	10%	38.79	8.57	3.88		17.83		27.52	3.15			73.34
	20%	34.01	16.74	3.44		18.86		22.13	4.55			67.66
	30%	29.72	25.21	3.08		18.98		16.98	5.75			61.45
	40%	25.86	33.69	2.75		18.37		12.46	6.59			54.73
	50%	22.25	42.21	2.42		17.14		8.74	6.97			47.61
	F=30	0%	45.91	0.28	2.90	14.54		34.95	1.19			81.08
	10%	41.92	4.66	3.05		17.10		30.93	2.08			76.33
F=40	20%	38.54	8.88	3.05		19.31		27.02	2.92			71.37
	30%	35.54	13.07	3.00		21.21		23.19	3.69			66.09
	40%	32.72	17.50	2.95		22.72		19.38	4.42			60.33
	50%	30.16	21.94	2.88		23.82		15.84	5.03			54.23
	F=50	0%	46.78	0.19	2.19	13.33		36.33	0.97			82.93
	10%	43.71	3.14	2.42		15.79		33.09	1.61			78.88
	20%	40.86	6.07	2.57		18.25		29.74	2.23			74.39
F=30	30%	38.26	9.00	2.65		20.59		26.39	2.83			69.55
	40%	35.87	11.93	2.69		22.74		23.08	3.38			64.40
	50%	33.68	14.85	2.71		24.69		19.86	3.87			58.91
	F=40	0%	47.43	0.14	1.75	12.20		37.45	0.82			84.55
	10%	44.84	2.41	2.02		14.60		34.55	1.35			80.84
	20%	42.40	4.63	2.20		17.00		31.66	1.85			76.85
	30%	40.09	6.87	2.33		19.41		28.68	2.33			72.48
F=50	40%	37.99	9.03	2.41		21.72		25.77	2.77			67.90
	50%	36.02	11.19	2.47		23.98		22.84	3.18			62.93
	F=30	0%	46.09	0.11	1.39	11.67		39.85	0.69			85.88
	10%	45.70	1.95	1.73		13.51		35.70	1.18			82.48
	20%	43.59	3.73	1.91		15.75		33.19	1.59			78.98
	30%	41.56	5.49	2.06		18.05		30.59	1.99			75.14
	40%	39.55	7.32	2.18		20.45		27.83	2.38			70.81
F=40	50%	37.74	9.04	2.25		22.76		25.17	2.73			66.34

obvious as the case of adding IBC to the deep lunar mantle (Fig. 1d).

At the same depth, the effect on decreasing melting temperature of lunar mantle cumulate by adding IBC/KREEP becomes slightly less significant as the degree of partial melting increases, and this is somewhat more pronounced at deeper lunar mantles, e.g., the addition of 50 wt% of IBC to the deeper mantle causes the melting temperature of the lunar mantle cumulate to decrease by 253 °C for 5 wt% partial melting while 50 wt% of IBC can reduce the melting temperature by only 117 °C when the melting degree is about 50 wt% (Fig. 1c), compared with the primitive lunar mantle. In the shallow level of the lunar mantle, however,

this effect appears to disappear. At a constant mixing ratio of 50 wt% IBC, the reduction in melting temperature observed for 20 wt% partial melting compared to the primitive lunar mantle cumulate is approximately 70 °C. This reduction is comparable to the decrease observed for 50 wt% partial melting under the same mixing conditions (Fig. 1a).

3.2 The changes in lunar mantle constitution caused by lunar mantle overturn

Adding IBC/KREEP back to the lunar mantle will also cause changes in the mineral component of the lunar mantle. For example, adding IBC to the upper lunar mantle will increase

Table 6 Thermodynamic calculation results of melting temperatures (°C), residual solids compositions (wt%), densities (g/cm³), and melt densities for the Lin et al. (2017) mantle cumulate at ~120 km (0.6 GPa) within the lunar mantle with varying IBC fractions and degrees of partial melting (Sp. Spinel; Cpx. clinopyroxene; Opx. Orthopyroxene; Ol-Olivine)

Melt Frac.	IBC Frac.	ρ_{melt}	ρ_{solid}	$\Delta\rho$	T _{melting}	Sp	Cpx	Opx	Ol	Fe–Ti oxide
F=5	0%	2.95	3.26	0.317	1254	0.00	25.96	63.99	10.06	0.00
	10%	3.12	3.28	0.166	1225	0.00	28.06	63.19	8.75	0.00
	20%	3.21	3.30	0.091	1214	1.62	30.97	61.46	5.95	0.00
	30%	3.21	3.32	0.118	1219	4.43	31.37	62.51	1.68	0.00
	40%	3.29	3.35	0.055	1202	5.57	33.25	61.17	0.00	0.00
	50%	3.37	3.37	-0.002	1180	3.97	40.90	54.43	0.00	2.28
F=10	0%	2.93	3.26	0.330	1264	0.00	4.68	83.52	11.80	
	10%	3.04	3.28	0.239	1242	0.00	8.99	80.95	10.06	
	20%	3.14	3.29	0.148	1226	0.00	14.02	76.99	8.99	
	30%	3.19	3.31	0.128	1223	2.25	19.07	73.47	5.21	
	40%	3.18	3.33	0.151	1228	4.90	16.37	77.59	1.14	
	50%	3.24	3.35	0.116	1217	5.74	25.82	68.44	0.00	
F=20	0%	2.90	3.24	0.335	1309	0.00	0.00	84.25	15.75	
	10%	2.98	3.26	0.280	1288	0.00	0.00	86.70	13.30	
	20%	3.05	3.27	0.226	1271	0.00	0.00	88.55	11.45	
	30%	3.11	3.29	0.175	1256	0.00	0.00	90.02	9.98	
	40%	3.18	3.30	0.127	1242	0.00	0.00	91.15	8.85	
	50%	3.19	3.33	0.143	1242	3.34	0.00	93.23	3.43	
F=30	0%	2.88	3.22	0.337	1343	0.00	0.00	79.51	20.49	
	10%	2.94	3.24	0.295	1325	0.00	0.00	82.53	17.47	
	20%	3.00	3.25	0.253	1308	0.00	0.00	85.25	14.75	
	30%	3.05	3.27	0.213	1293	0.00	0.00	87.51	12.49	
	40%	3.10	3.28	0.176	1280	0.00	0.00	89.37	10.63	
	50%	3.16	3.30	0.140	1267	0.00	0.00	90.97	9.03	
F=40	0%	2.87	3.21	0.342	1369	0.00	0.00	72.99	27.01	
	10%	2.91	3.22	0.307	1352	0.00	0.00	77.04	22.96	
	20%	2.96	3.23	0.272	1337	0.00	0.00	80.50	19.50	
	30%	3.01	3.25	0.238	1322	0.00	0.00	83.81	16.19	
	40%	3.05	3.26	0.205	1309	0.00	0.00	86.55	13.45	
	50%	3.10	3.27	0.173	1296	0.00	0.00	89.03	10.97	
F=50	0%	2.85	3.20	0.351	1388	0.00	0.00	63.73	36.27	
	10%	2.89	3.21	0.320	1373	0.00	0.00	68.87	31.13	
	20%	2.93	3.22	0.290	1359	0.00	0.00	73.56	26.44	
	30%	2.97	3.23	0.258	1345	0.00	0.00	78.15	21.85	
	40%	3.02	3.24	0.228	1332	0.00	0.00	82.16	17.84	
	50%	3.06	3.25	0.199	1320	0.00	0.00	85.67	14.33	

the proportion of clinopyroxene and slightly decrease the proportion of olivine (Fig. 2a, b), but clinopyroxene will almost disappear if a large degree (> 20 wt%) of partial melting happens, in which case the proportion of orthopyroxene increases (Fig. 2c, d, e, f). For the case that the degree of partial melting is no more than 10 wt%, the calculation results show the appearance of other mineral phases besides olivine and pyroxene, such as spinel when the fraction of IBC is greater than 20 wt%, and Fe–Ti oxide appears when the F=5 and the IBC content greater than 40 wt%. The formation of spinel or Fe–Ti oxide can explain the sharp changes in melting temperature mentioned above (Fig. 1). Mixing KREEP with the upper lunar mantle cumulate shows

very different effects on the constitution of the lunar mantle cumulate. For example, the proportion of clinopyroxene largely increases even after the large degree of partial melting, and adding more KREEP will largely decrease the proportion of orthopyroxene and olivine in the upper lunar mantle (Fig. S1). For the cases where the degree of partial melting is less than 20 wt%, the residual solid mantle contains some amount of plagioclase (~1 wt%–10 wt%, Fig. S1a, b, c), which again can explain the unusual melting temperature changes present in Fig. 1. For the case that the KREEP proportion is larger than 20 wt%, the modified lunar upper mantle will be dominated by clinopyroxene if the melting degree is no more than 20 wt%, which will also

Table 7 Thermodynamic calculation results of melting temperatures (°C), residual solids compositions (wt%), densities (g/cm³), and melt densities for the Lin et al. (2017) mantle cumulate at ~420 km (2 GPa) within the lunar mantle with varying IBC fractions and degrees of partial melting (Sp-Spinel; Cpx-clinopyroxene; Opx-Orthopyroxene; Ol-Olivine)

Melt Frac.	IBC Frac.	ρ_{melt}	ρ_{solid}	$\Delta\rho$	T _{melting}	Sp	Cpx	Opx	Ol	
F=5	0%	3.061	3.171	0.110	1583	0.00	0.00	18.33	81.67	
	10%	3.230	3.207	-0.023	1509	0.00	0.00	25.70	74.30	
	20%	3.380	3.240	-0.140	1451	0.00	0.00	32.39	67.61	
	30%	3.543	3.277	-0.266	1380	0.00	0.00	39.00	61.00	
	40%	3.748	3.317	-0.432	1294	0.00	0.76	45.14	54.11	
	50%	3.646	3.344	-0.302	1330	4.57	0.00	55.90	39.54	
	F=10	0%	3.047	3.162	0.116	1597	0.00	0.00	16.58	83.42
		10%	3.168	3.193	0.025	1541	0.00	0.00	24.59	75.41
		20%	3.276	3.223	-0.053	1496	0.00	0.00	31.98	68.02
		30%	3.378	3.253	-0.125	1455	0.00	0.00	39.09	60.91
		40%	3.475	3.285	-0.191	1414	0.00	0.00	46.10	53.90
	F=20	50%	3.575	3.317	-0.257	1369	0.00	0.00	53.16	46.84
		0%	3.023	3.151	0.128	1611	0.00	0.00	12.64	87.36
		10%	3.111	3.175	0.064	1572	0.00	0.00	21.92	78.08
		20%	3.194	3.200	0.006	1537	0.00	0.00	30.70	69.30
		30%	3.274	3.225	-0.049	1504	0.00	0.00	39.22	60.78
	F=30	40%	3.353	3.252	-0.101	1471	0.00	0.00	47.50	52.50
		50%	3.430	3.280	-0.150	1439	0.00	0.00	55.62	44.38
		0%	3.003	3.143	0.140	1619	0.00	0.00	7.47	92.53
		10%	3.072	3.162	0.090	1590	0.00	0.00	18.00	82.00
		20%	3.144	3.183	0.039	1561	0.00	0.00	28.63	71.37
	F=40	30%	3.215	3.204	-0.011	1532	0.00	0.00	38.90	61.10
		40%	3.287	3.227	-0.060	1503	0.00	0.00	48.84	51.16
		50%	3.357	3.250	-0.106	1474	0.00	0.00	58.56	41.44
		0%	2.985	3.137	0.152	1625	0.00	0.00	0.00	100.00
		10%	3.046	3.154	0.108	1601	0.00	0.00	12.80	87.20
	F=50	20%	3.107	3.170	0.063	1577	0.00	0.00	25.49	74.51
		30%	3.171	3.188	0.017	1552	0.00	0.00	37.97	62.03
		40%	3.234	3.206	-0.028	1527	0.00	0.00	50.09	49.91
		50%	3.299	3.225	-0.074	1501	0.00	0.00	62.01	37.99
		0%	2.992	3.128	0.135	1639	0.00	0.00	0.00	100.00
	F=60	10%	3.024	3.147	0.124	1609	0.00	0.00	5.19	94.81
		20%	3.077	3.161	0.084	1589	0.00	0.00	20.50	79.50
		30%	3.133	3.175	0.042	1568	0.00	0.00	35.97	64.03
		40%	3.193	3.190	-0.003	1545	0.00	0.00	51.16	48.84
		50%	3.252	3.204	-0.048	1522	0.00	0.00	66.03	33.97

be true for the larger degree of partial melting if the mixture contains more than 30 wt% KREEP (Fig. S1).

Adding IBC to the lower lunar mantle always causes some increment in the content of orthopyroxene and decreases the proportion of olivine and the degree of partial melting does not show the effect on the trend except that a small amount of spinel can retain in the residual solid lunar mantle if the melting degree is about 5 wt% (Fig. 3). On the other hand, mixing varying amounts of KREEP with the primitive lower lunar mantle cumulate produces distinct changes in mineral composition, potentially introducing clinopyroxene to the lower mantle. For the case that the degree of partial melting is only 5 wt%, garnet appears as a stable phase in the

residual solid mantle cumulate, and for a relatively large degree of partial melting, spinel shows up accompanied by increasing clinopyroxene and decreasing orthopyroxene and olivine content in the modified lunar mantle cumulate (Fig. S2).

3.3 Properties of the silicate melt generated through partial melting of lunar mantle cumulates mixed with IBC/KREEP

There are some general trends in the chemical composition of silicate melt that are generated by partial melting of lunar mantle cumulates mixed with IBC/KREEP. Adding

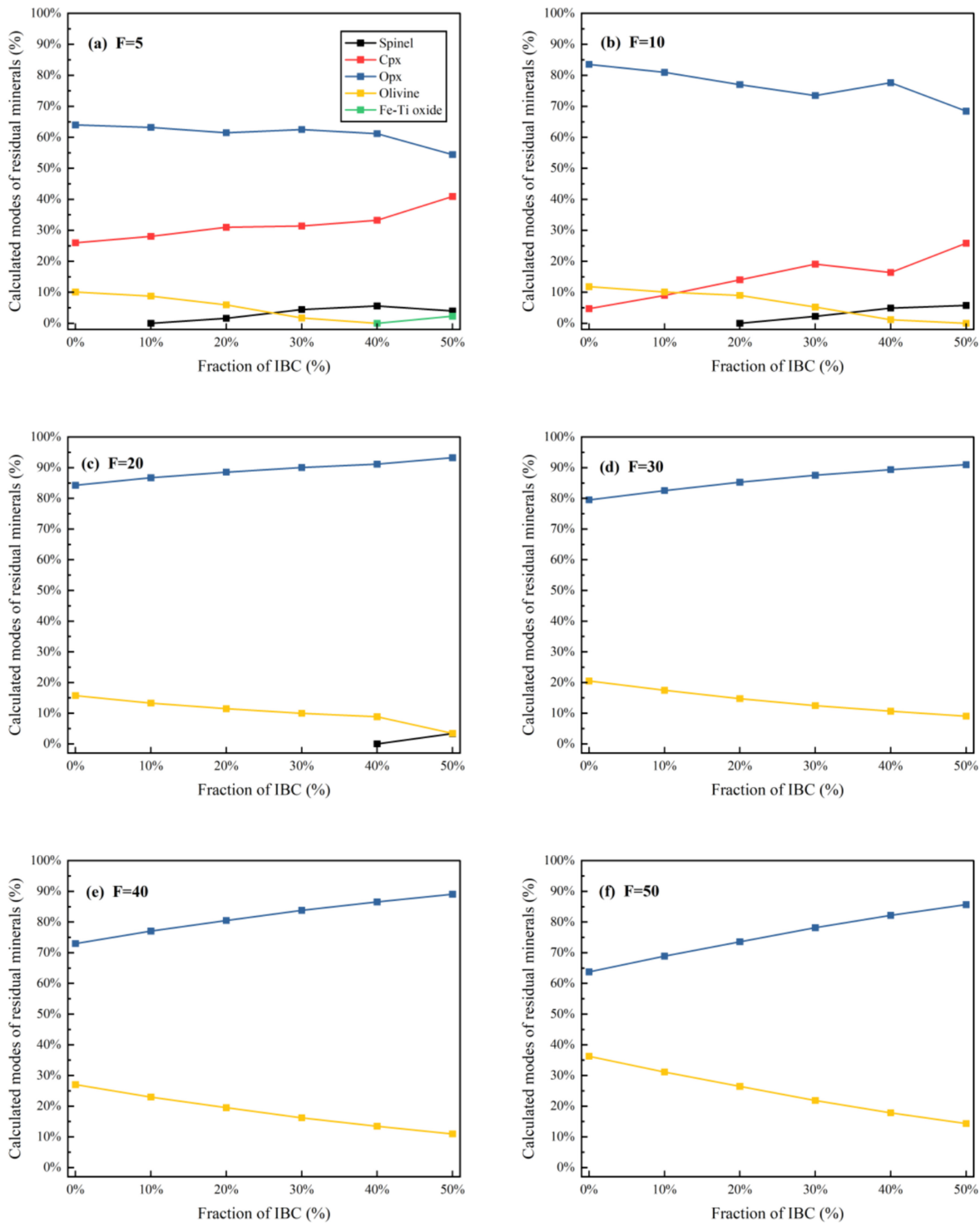


Fig. 2 Mineral assemblages of the residual solids for IBC mixed with mantle cumulates at 0.6 GPa for different degree of partial melting (F) up to 50 wt%

more materials from late LMO differentiation to the lunar mantle will generate silicate melt with higher FeO and TiO₂ content and lower MgO content for the degree of partial melting from 5 wt% to 50 wt%. High-Ti silicate melt can

be generated if the proportion of IBC in the mixture is as large as 30 wt% or for a relatively small degree of partial melting (e.g., ≤ 30 wt%, Figs. 4 and 5). With increasing content of IBC in the mixed upper lunar mantle, the CaO

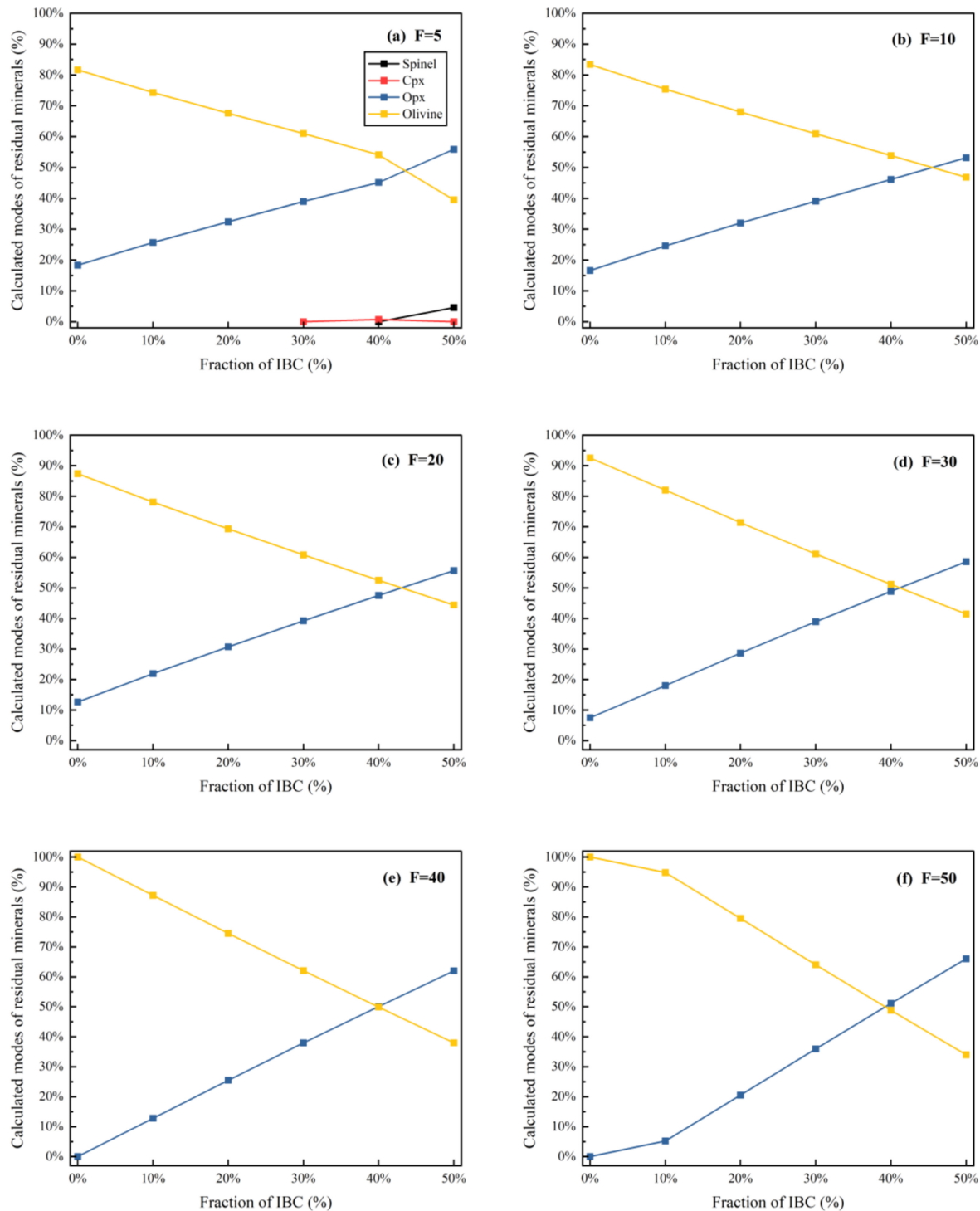


Fig. 3 Mineral assemblages of the residual solids for IBC mixed with mantle cumulates at 2 GPa for different degree of partial melting (F) up to 50 wt%

content of silicate melts remains almost unchanged, while the Al_2O_3 content decreases slightly, the MgO content decreases sharply, and the TiO_2 and FeO contents increase significantly (Fig. 4). In contrast, melts generated by lunar upper mantle hybridizing with KREEP show that only MgO

content decreases while TiO_2 , Al_2O_3 , and CaO contents increase with increasing proportion of KREEP in the mixture. Their FeO content increases for the situations where the proportion of KREEP in the mixture is less than 30 wt% and then decreases if more KREEP is added to the lunar mantle

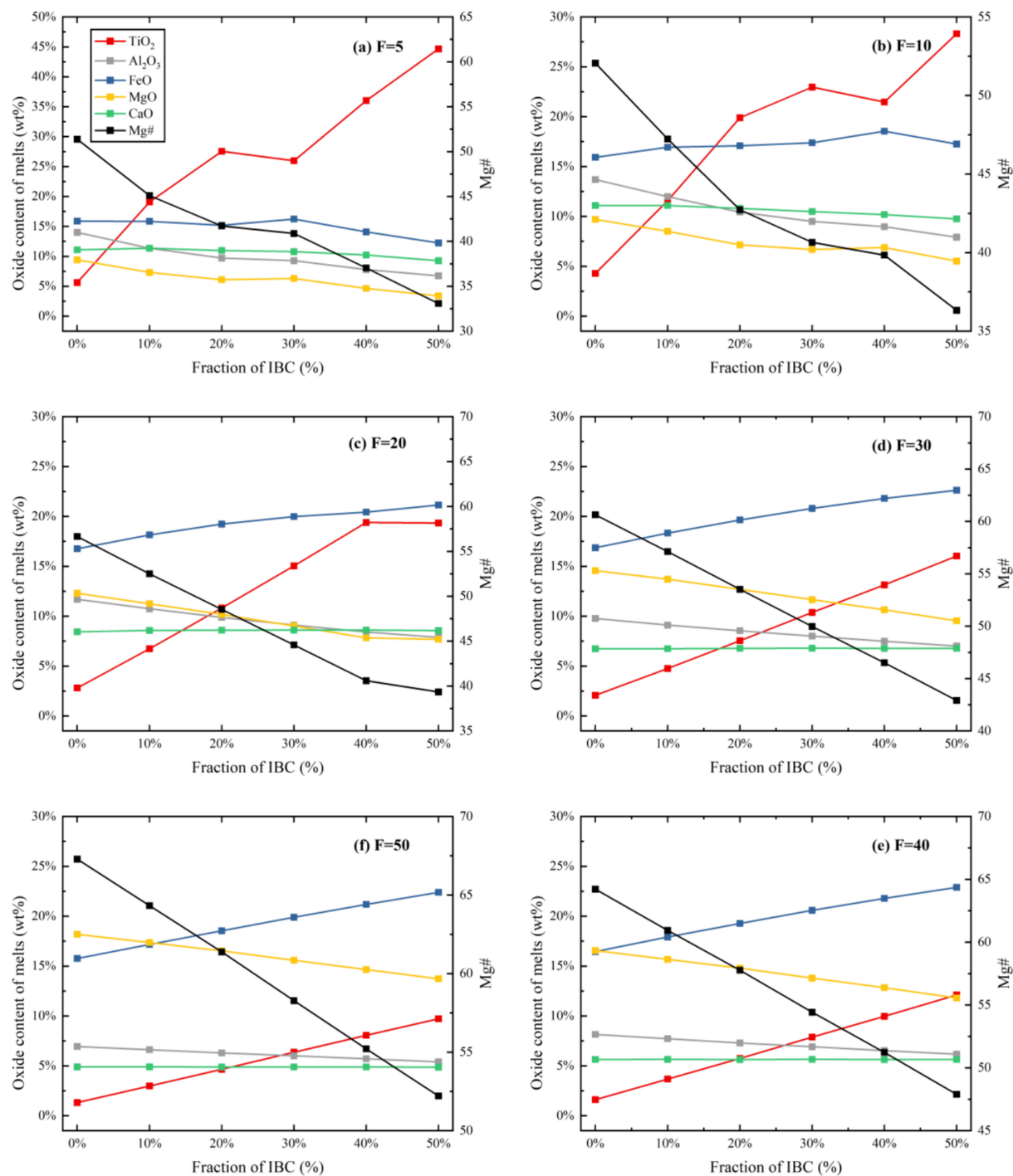


Fig. 4 Compositions of silicate melt formed through partial melting of IBC mixed cumulates at 0.6 GPa for different degree of partial melting (F) up to 50 wt%

cumulates (Fig. S3). Similarly, adding more IBC to the lower lunar mantle will generate silicate melts with high TiO₂ concentrations up to 8 wt%–60 wt% if the proportion of IBC in the mixture is as high as 50 wt%. For the case that only 10 wt% IBC was added to the mixture, the TiO₂ content in the silicate melt can still be as high as about 10 wt% if the partial

melting degree is not larger than 10 wt%. The melt with high TiO₂ content also shows characteristics of relatively high FeO concentrations (Fig. 5). The silicate melts generated by adding different amounts of KREEP to the lower lunar mantle also show similar trends in their chemical compositions (Fig. S4). Generally, with increasing amounts of KREEP in

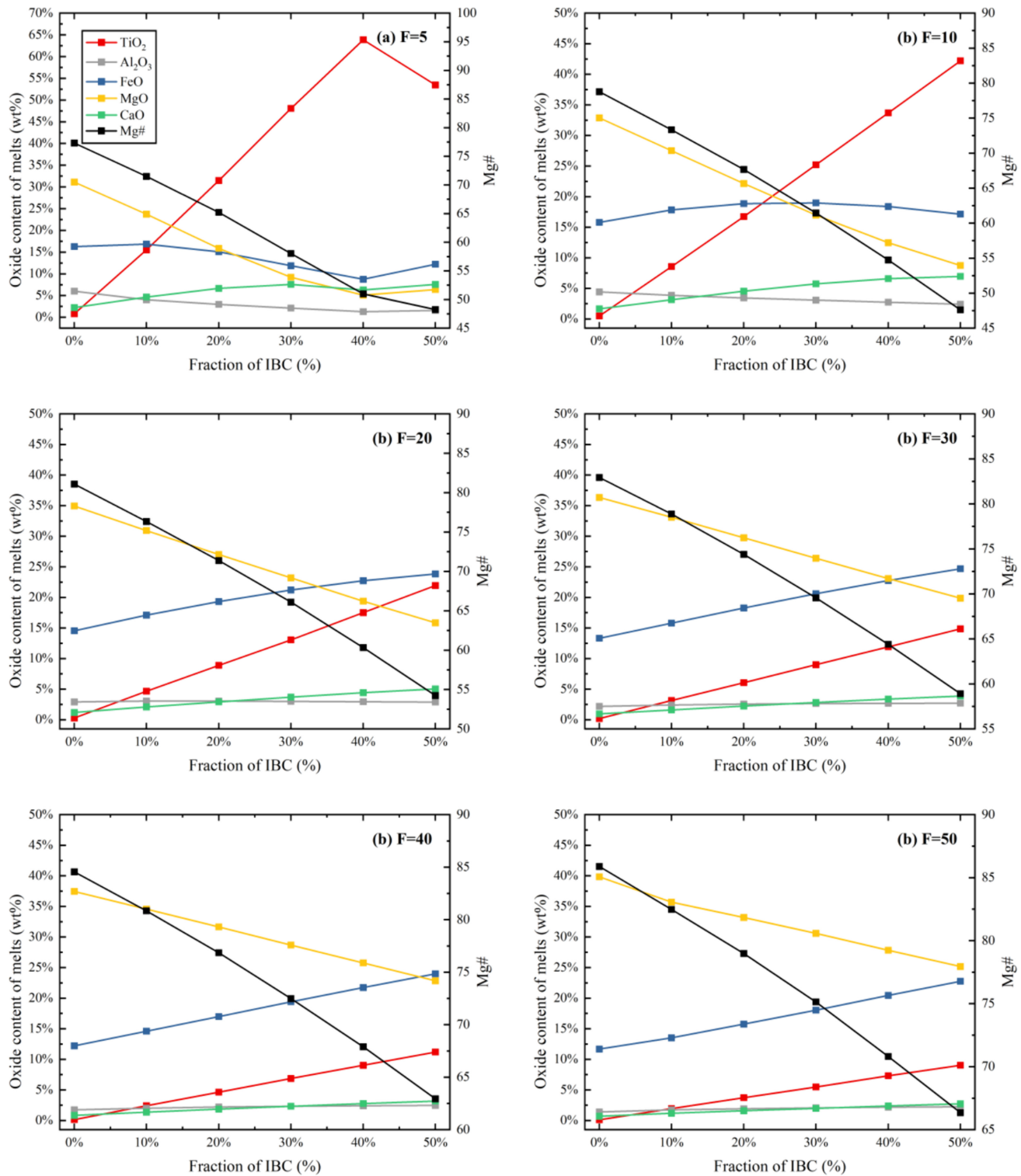


Fig. 5 Compositions of silicate melt formed through partial melting of IBC mixed cumulates at 2.0 GPa for different degree of partial melting (F) up to 50 wt%

the mixture, the silicate melts show higher FeO , TiO_2 , CaO , and Al_2O_3 concentrations. For the case with a relatively low degree of partial melting (<20 wt%), there are some changes

in the trends of the chemical compositions of silicate melts, such as their CaO and Al_2O_3 contents increase as the proportion of KREEP increase and then gradually decrease (Fig.

S4), which is corresponding to the stability of spinel in the residual solid lunar mantle (Fig. S2).

4 Discussion

4.1 The extent of partial melting of IBC/KREEP-bearing cumulates at different depths of lunar mantle

The hypothesis of partial melting occurring within mantle cumulates during lunar mantle overturn has some important implications such as explanations for the dynamic stability of Ti-bearing cumulates at CMB (e.g., Dygert et al. 2016; Jacobs et al. 2022; Zhang et al. 2017; Zhao et al. 2019), the unusual low seismic velocities (Nakamura 2005; Weber et al. 2011) and viscosity (Harada et al. 2014), and high electrical conductivity (Khan et al. 2014) of lunar mantle materials at CMB (e.g., Garcia et al. 2019; Harada et al. 2014; Khan et al. 2014; Nakamura 2005; Pommier et al. 2024; van Kan Parker et al. 2012; Weber et al. 2011; Xu et al. 2022). These scenarios assume that the high-density IBC can directly sink to the lowermost lunar mantle although melt-induced viscosity reduction is needed for decoupling IBCs from the top stagnant lid (e.g., Li et al. 2019). In other words, the extent of partial melting of lunar mantle cumulate during overturn is very restricted.

On the other hand, lunar magma ocean differentiation models have suggested that IBC and KREEP are characterized by lower melting temperatures compared to other lunar mantle cumulates formed deep inside the Moon (e.g., Ju et al. 2022; Lin et al. 2017; Rapp and Draper 2018; Snyder et al. 1992), implying that during sinking, IBC/KREEP may get heated and become thermodynamically unstable. In other words, partial melting may happen during the downwelling of IBC/KREEP. The solidi and the extent of partial melting of mixed lunar mantle cumulates largely depend on the lunar mantle thermal condition and the composition of the mixed lunar mantle cumulates as the calculation results from this study show that the melting temperature of the mixed lunar mantle cumulates changes with the proportion of IBC/KREEP (Fig. 1). Due to the absence of information about the thermal condition deep inside the Moon during the lunar mantle overturn, we consider two reference temperature gradients based on: (1) experiments and numerical simulations on LMO crystallization (e.g., Ju et al. 2022; Lin et al. 2017; Rapp and Draper 2018; Schmidt and Kraettli 2022), and (2) geophysical data interpretations and inverse modeling on the present-day lunar mantle properties (Hood et al. 1982; Karato 2013; Khan et al. 2014; Zhang et al. 2019). At the early stage of LMO differentiation, the Moon continuously released heat directly to the cold space through the magma ocean, leading to a gradual cooling Moon. However, upon the onset of plagioclase

crystallization and the subsequent formation of an anorthitic flotation crust overlying the magma ocean, the presence of this stagnant anorthositic crust significantly inhibits the cooling of the LMO (Elkins-Tanton et al. 2011). It is reasonable to assume that the temperature inside the Moon at the ending stage of LMO differentiation is much higher than those estimated based on geophysical parameters, that resemble the current condition inside the Moon, but rather close to the temperature conditions used in LMO modeling. Thermodynamic calculation results from this study revealed that the presence of IBC/KREEP lowers solidi temperature of lunar mantle cumulates. By adding 50 wt% of IBC, the melting temperature of the mixture is as low as ~1180 °C at 0.6 GPa (120 km) and it is ~1330 °C at 2 GPa (~420 km). Applying the calculated melting temperature of the mixed lunar mantle cumulates to the geotherm of the early Moon, in the shallow lunar mantle, assuming a thermal gradient approximating that calculated by Ju et al. (2022) (700 km LMO Model) and a high mixing efficiency between IBC/KREEP and lunar mantle cumulates, partial melting degrees of up to 50 wt% can be achieved for cumulates with 50 wt% IBC content, while for cumulates

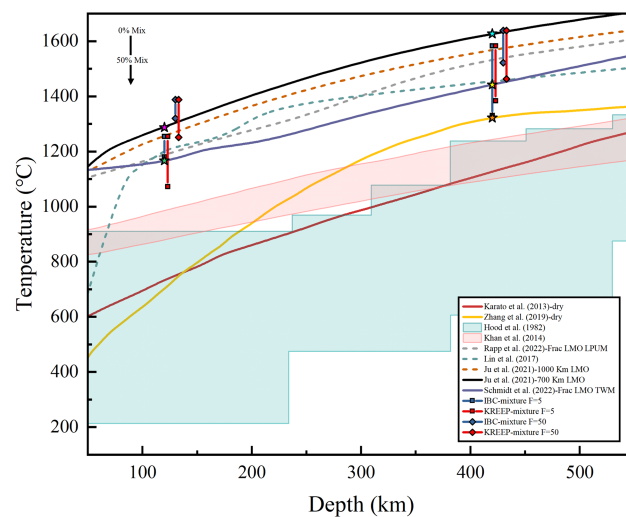


Fig. 6 Comparison of the melting temperature of IBC/KREEP-mixture with lunar mantle geotherms. The melting temperatures of the IBC/KREEP mixture are shown in blue/red solid lines with square markers (5 wt% melting) and diamond markers (50 wt% melting). The black solid line (Ju et al. 2022) and the purple solid line (Schmidt et al. 2022) represent two different lunar mantle geotherms determined by experiments or numerical simulations on LMO fractionation. The temperature at ~120 km depth is estimated to be ~1160 °C for colder geotherm (green star, as the 5 wt% partial melting temperature of 1166 °C for 30 wt% KREEP-mixture) and ~1280 °C for hotter geotherm (red star). Similarly, the temperature for colder and hotter geotherms at ~420 km depth are estimated to be ~1440 °C (yellow star, as the 5 wt% partial melting temperature of 1451 °C for 20 wt% IBC-mixture) and ~1630 °C (blue star), respectively. Notably, the current highest estimation for the lunar mantle temperature at ~420 km depth is indicated by the orange star as ~1320 °C, which is nearly equal to the 5 wt% partial melting temperature of a 50 wt% IBC-mixture

containing 10 wt% IBC, the melting degree is estimated to be 30 wt% (Fig. 6). If we took the relatively cooler geotherm, then the solidus of mantle cumulate at 120 km with 50 wt% IBC is close to the temperature predicted by Schmidt and Kraettli (2022), in which case, the degree of partial melting is no more than 5 wt%. For the case to mix mantle cumulate with KREEP, the solidus of the mixture is about 100 °C lower than the case mixed with IBC, thus larger degree of partial melting will happen during overturn. Similarly, compared to our calculation results at 2 GPa with different geotherms, the solidi of mantle cumulates with different amounts of IBC/KREEP are lower than the mantle temperature at 420 km. This suggests a greater degree of partial melting at depth compared to the shallower mixed lunar mantle. In an extreme case, mixing the deep lunar mantle cumulates with 50 wt% IBC, the temperature for 5 wt% partial melting is only 1330 °C, close to the present-day lunar mantle temperature proposed by Zhang et al. (2019) (Fig. 6). Along this line, we propose that partial melting could occur in different depths (> 120 km) of the lunar mantle during the sinking of IBC/KREEP. This assumption is strengthened when considering the more realistic scenario of IBC and KREEP co-subsidence, coupled with the transport of heat-producing elements K, U, and Th would be carried into the lunar interior and heating the IBC/KREEP during sinking, thereby facilitating partial melting of the mixed cumulate.

Given the LMO model (Lin et al. 2017) that we have chosen for this study, the shallow lunar mantle (~ 120 km) exhibits an olivine (11%) + clinopyroxene (89%) mineral assemblage, consistent with some other LMO models (e.g., Rapp and Draper 2018). However, the deeper lunar mantle (~ 420 km) is characterized by a harzburgite layer with 25% orthopyroxene in addition to olivine (75%), while other models exhibit a dunite layer (e.g., Snyder et al. 1992). The abundance of orthopyroxene in the deeper lunar mantle may result in a lower solidus in the deeper lunar mantle (2 GPa), leading to a larger degree of partial melting compared to other LMO models. Moreover, given the different effects of KREEP and IBC on the solidi of mixed lunar mantle cumulates, KREEP and IBC may have been decoupling before they sink to deeper lunar mantle if the degree of partial melting is large enough for all the incompatible elements carried by KREEP to partitioning to the silicate melt. If this is what happened to KREEP during mantle overturn, then there will be no radioactive heat to trigger partial melting of the lower lunar mantle.

4.2 Characteristics and distribution of melt induced by mixing lunar mantle cumulates with IBC/KREEP

If the sinking of IBC/KREEP during lunar mantle overturn triggered partial melting of the primordial lunar mantle cumulates, the resulting melts are likely to be characterized

by high-Ti content and high density, necessitating consideration of their distribution behavior within the lunar mantle. The ability of melts to undergo buoyancy-driven separation from residual solid phases largely depends on the density contrast ($\Delta\rho$) between the liquid and the surrounding residual solid mantle rather than viscosity, as melt viscosity is vastly higher than that of the solid phase (Hess and Parmentier 1995; Spera 1992). As estimated by Hess and Parmentier (1995) in their study of lunar mantle overturn dynamics, the reasonable minimum viscosity of solid mafic lunar mantle near its melting temperature is 10^{19} Pa·s, which is far greater than the maximum viscosity of even high-Ti Apollo picritic black glass below its liquidus (~ 0.9 Pa·s, Delano 1990). Therefore, only in the dynamics of solid–solid phases does the viscosity difference between solid phases become a nearly decisive parameter, determining whether and to what extent separation can occur (Elkins-Tanton et al. 2011; Li et al. 2019; Zhao et al. 2019). This study considers only the density contrast as the primary driving factor for the buoyancy-driven migration of silicate melts. If the density of silicate melts is greater than that of the surrounding lunar mantle material, they will sink to greater depths within the Moon, possibly reaching the CMB. Conversely, if the melt density is less than that of the residual solid mantle cumulates, the silicate melts may rise to the crust–mantle boundary, or even erupt through fractures in the lunar crust, forming various types of lunar igneous rocks on the surface.

The gravitational stabilities of the silicate melt generated during the partial melting of mixed mantle cumulates are evaluated by comparing the calculated density of the melt with the density gradient of the surrounding lunar mantle and the residual lunar mantle solidus. To illustrate the extreme case (only 5 wt% degree of partial melting), we compared the densities of melts generated from different mixtures by varying the proportion of IBC/KREEP (0 wt%–50 wt%) to the density of the surrounding lunar mantle at the corresponding depth. By adding different amounts of IBC to the upper lunar mantle and generating 5 wt% melt, the density difference between residual solid mantle and silicate melt ranges from 0.317 g/cm³ (0 wt% IBC) to –0.002 g/cm³ (50 wt% IBC) (Table 6). These melts can be considered to be positively buoyant. It is important to note that as the degree of partial melting increases, the density of either the residual solid mantle or the melt will gradually decrease but the density difference between the two phases increases (Fig. 7). As the degree of partial melting increases, the melt density lines will shift slightly to the left in Fig. 8. Although there are some increments in density as the amount of IBC or KREEP in the mixed cumulates increases, the densities of both groups of melts are all lower than the lunar mantle at shallow depth (0.6 GPa, ~ 120 km) (Fig. 8), therefore, silicate melts will be positively buoyant concerning the surrounding mantle. For the cases

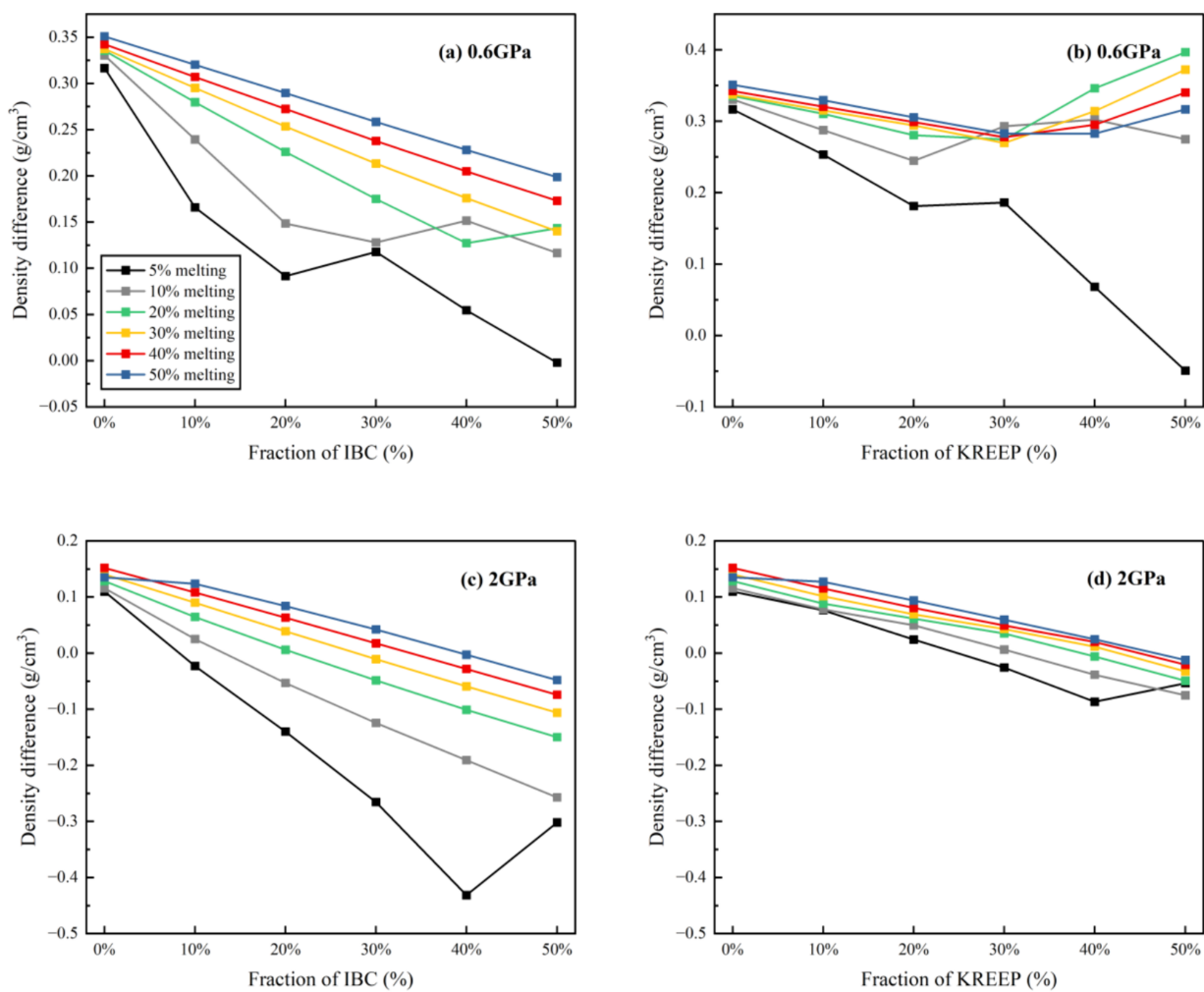


Fig. 7 Density differences between solid residual and silicate melts under two different pressure conditions. **a** IBC mixture and **b** KREEP mixture at 0.6 GPa; **c** IBC mixture and **d** KREEP mixture at 2 GPa

where 5 wt% melt was generated from partial melting of the mixed mantle cumulates with 50 wt% IBC/KREEP, the melt density approaches the higher limit of the selected lunar mantle density gradient (Fig. 8, Khan et al. 2014). For the same amount of melt, adding more high-density materials such as IBC to the lunar mantle cumulates will balance out the density difference between the liquid and the residual mantle solid, thus making the liquid less buoyant. For large degrees of partial melting such as 20 wt%, the smallest density difference (50 wt% of IBC in the mixture) is about 0.15 g/cm³ (Fig. 7), suggesting upward movement of the high-Ti silicate melt. We should also mention that there are some cases that the density of melt is close to that of the surrounding lunar mantle, making them neutral buoyancy, which may crystallize to form ilmenite or armalcolite during continuous cooling as suggested by Thacker et al. (2009).

In contrast, within the deep lunar mantle (2 GPa, ~420 km), the density of partial melts generated by mixing

lunar mantle cumulates with varying proportions of IBC/KREEP exhibits a significant increase compared to those derived from the shallow mantle, while the density of solid mantle material does not show large variation (Tables 6 and 7). To illustrate, consider the scenario of 5 wt% partial melting as a representative case, the density of melt increases from 3.06 to 3.38 g/cm³ as the proportion of IBC in the mixture increases to 20 wt%, in which case the density of the residual mantle is only 3.24 g/cm³ (Fig. 8). The calculation results suggest that less than 10 wt% melt generated by adding more than 20 wt% IBC to the deep lunar mantle cumulates will make silicate liquid denser than the surrounding mantle. Thus, these melts may be negatively buoyant within the lunar interior and sink to the CMB where they remain as a partially molten layer until the present day. It is noteworthy that for higher melt fractions, a greater mixing degree is required to achieve the mentioned density range. However, when the melt fraction exceeds 40 wt%, even a

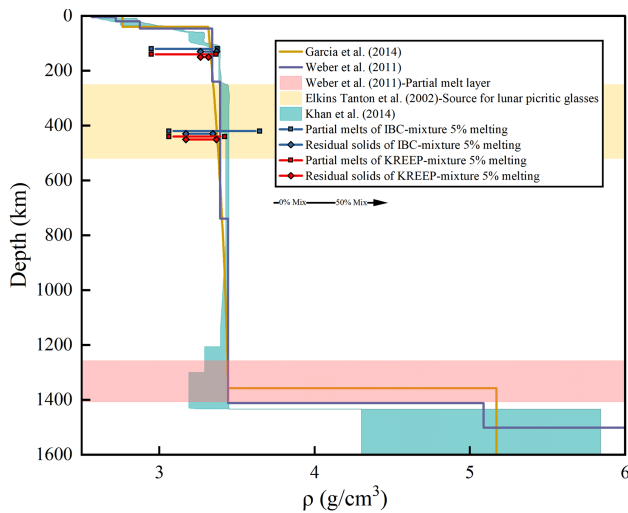


Fig. 8 Comparison of the density of Fe–Ti/KREEP-rich melts with corresponding residual solids and the lunar density gradient from different models (Garcia et al. 2012; Weber et al. 2011; Khan et al. 2014). The density of melt derived from 5 wt% partial melting of the IBC/KREEP mixture (blue/red solid lines with square markers) is compared with the surrounding rock (the blue/red solid lines with diamond markers for residual solid of IBC/KREEP-mixture) and the recent lunar seismic models at two depths. The solid lines depict the density increasing from 0 wt% addition at the left endpoint to 50 wt% addition at the right endpoint, indicating a positive correlation between density and increasing degree of mixing

mixing degree as high as 50 wt% cannot produce a density sufficient for the melt to sink (Fig. 8). On the other hand, for the cases where the IBC content in the deep mixed lunar mantle cumulate is less than 20 wt% and the degree of partial melting is over 30 wt%, the density difference between the solid and the silicate melt is positive, suggesting upward migration of the silicate melt. However, this situation also indicates a much hotter lunar interior environment. At this depth, almost all the calculated KREEP-bearing melts are less dense than the surrounding lunar mantle. To keep the KREEP-bearing melts deep inside the lunar mantle will require comparable density between the solid and the liquid phase, thus small degree of melting with a large amount of KREEP in the mixture is needed, indicating a relatively cold mantle.

Due to the large discrepancy in density between KREEP-bearing melt and IBC-bearing melt, the two components may separate during partial melting in the lunar mantle (Tables 6, 7, S3, and S4). If partial melting happens at the upper lunar mantle during mantle overturn, both KREEP-bearing and IBC-bearing melt are much less dense than the surrounding lunar mantle and, thus will move upward. For the cases where a large amount of IBC/KREEP (> 30 wt%) was added to the mantle cumulates but only a small degree of partial melting (< 20 wt%) happened, the density of IBC-bearing melt is comparable with the solid mantle, but

KREEP-bearing melt is much less in density, and considering the lower melting temperature of KREEP-mixtures compared to IBC-mixtures, thus these two different kinds of liquid phases may separate. For the cases where partial melting happened deep inside the Moon (2 GPa, ~420 km), the densities of KREEP-bearing melts are not significantly different compared with the residual solid mantle, therefore most likely remain inside the Moon. As mentioned above, IBC-bearing melt may downward migration if a large amount of IBC is mixed with mantle cumulate and causes less than 20 wt% melting, in which case the KREEP-bearing melt may separate from IBC-bearing melt (Fig. 7). Based on the thermodynamic calculation present in this study, if partial melting happens during the lunar mantle overturn, it is difficult for KREEP to be transferred to the lower lunar mantle. However, we simplify the process of lunar mantle overturn by calculating the effect of IBC and KREEP on the melting temperature of lunar mantle cumulates separately. According to LMO differentiation models, KREEP is only some drizzles of residual LMO that are attached to IBC. Therefore, if partial melting happens in the upper lunar mantle, KREEP-rich materials may move upward, and they may migrate downward together with IBC-bearing melt if a small degree of partial melting happens in a relatively deep mantle.

4.3 Constitution and structure of lunar mantle after overturn

An important petrological consequence of partial melting, and melt segregated from its source region driven by buoyancy is the change in the constitution and structure of the lunar mantle. As an example, we use the mineral proportions to represent the constitution of the lunar mantle at different depths. For the cases where partial melting happened in the upper lunar mantle, then after extraction of melt, the mantle composition will change from clinopyroxene dominant (89%) to orthopyroxene dominant (> 60%), and a certain amount of spinel will be contained inside the mantle if the degree of melting is less than 10 wt%. Some amount of Fe–Ti oxide will appear if the added IBC is large enough (> 40 wt%). This modified Ti-Fe-enriched lunar mantle can serve as a source region for elucidating the origin of high-Ti lunar basalt. The addition of KREEP to the upper lunar mantle will not only increase the proportion of orthopyroxene but also result in the formation of plagioclase. Such kind of modified lunar mantle may offer a potential explanation for the formation of high-Al basaltic magma in early Moon magmatic activities, and further investigation is encouraged to substantiate this hypothesis. Conventional LMO models assume that plagioclase floated up during LMO crystallization, forming the anorthositic crust. Even in the case of inefficient

flotation, only minuscule amounts of trapped melt could be present within crystal interstices, it is thus difficult to form an Al-rich magma through partial melting of lunar mantle cumulate formed through LMO differentiation. In this study, our investigation suggests that if significant KREEP downwelling occurs during lunar mantle overturn, partial melting of upper lunar mantle cumulates with the addition of KREEP will stabilize some Al-rich mineral phases such as plagioclase or spinel in the residual upper mantle and remelting such kind of mantle cumulates can form basaltic magma enriched with Al_2O_3 .

If IBC/KREEP sinks to the lower lunar mantle (~ 420 km) and causes a certain degree of partial melting, then after the extraction of these melts, the residual lunar mantle will change from olivine dominated dunite layer to a cumulate layer with olivine + orthopyroxene + clinopyroxene. The existence of a certain amount of clinopyroxene will lower the melting temperature of the lunar mantle. Moreover, if a substantial amount of Ti-Fe-rich components was retained in the residual solid phase following partial melting, it then crystallized ilmenite in the middle of the lunar mantle, making a hybrid heterogeneous mantle source, offering a good explanation for the relatively deeper source region for the lunar high-Ti volcanic glasses and low-Ti volcanic glass (Grove and Krawczynski 2009). On the other hand, if a relatively small degree of partial melting (< 20 wt%) happened at ~ 420 km during the sinking of IBC, then the large density of the melt will facilitate the downward percolation of high-Ti content material through the underlying mantle to the CMB eventually as suggested by geophysical interpretation (van Kan Parker et al. 2012).

5 Conclusions

- 1) Thermodynamic simulation on solidi of lunar mantle cumulates with IBC/KREEP shows that larger than 5 wt% degree of partial melting would happen if the IBC/KREEP layer sinks back to primitive lunar mantle crystallized from LMO.
- 2) The density difference between residual solid mantle and silicate melt decreases as the extent of partial melting increases. In most cases, the silicate melt is much less dense than the surrounding mantle in the shallow lunar mantle, thus will move upward, but the situation will be reversed in the lower lunar mantle.
- 3) The different degrees of partial melting and extraction of silicate melt will make large modifications to the primitive lunar mantle (e.g., The addition of IBC may lead to an orthopyroxene-dominated upper lunar mantle, while the addition of KREEP could introduce a certain amount of clinopyroxene to the lower lunar mantle).

Acknowledgements The authors thank the two anonymous reviewers for their constructive comments. This work was funded by the National Natural Science Foundation of China (41773052, 41973058).

Author contributions Wei Du contributed to the conception and design of the study; Wei Huang performed thermodynamic calculations; Wei Huang and Wei Du wrote and revised the manuscript draft.

Declarations

Conflict of interest The authors declare that they have no known competing financial interests or personal relationships that could have appeared to influence the work reported in this paper.

References

- Agee CB, Walker D (1993) Olivine flotation in mantle melt. *Earth Planet Sci Lett* 114(2):315–324. [https://doi.org/10.1016/0012-821X\(93\)90033-6](https://doi.org/10.1016/0012-821X(93)90033-6)
- Arai T, Maruyama S (2017) Formation of anorthosite on the Moon through magma ocean fractional crystallization. *Geosci Front* 8(2):299–308. <https://doi.org/10.1016/j.gsf.2016.11.007>
- Borg LE, Connelly JN, Boyet M, Carlson RW (2011) Chronological evidence that the Moon is either young or did not have a global magma ocean. *Nature* 477(7362):70–72. <https://doi.org/10.1038/nature10328>
- Borg LE, Gaffney AM, Shearer CK (2015) A review of lunar chronology revealing a preponderance of 4.34–4.38 Ga ages. *Meteorit Planetary Sci* 50(4):715–732. <https://doi.org/10.1111/maps.12373>
- Borg LE, Cassata WS, Wimpenny J, Gaffney AM, Shearer CK (2020) The formation and evolution of the Moon's crust inferred from the Sm-Nd isotopic systematics of highlands rocks. *Geochim Cosmochim Acta* 290:312–332. <https://doi.org/10.1016/j.gca.2020.09.013>
- Boukaré CE, Parmentier EM, Parman SW (2018) Timing of mantle overturn during magma ocean solidification. *Earth Planet Sci Lett* 491:216–225. <https://doi.org/10.1016/j.epsl.2018.03.037>
- Canup RM, Asphaug E (2001) Origin of the Moon in a giant impact near the end of the Earth's formation. *Nature* 412(6848):708–712. <https://doi.org/10.1038/35089010>
- Charlier B, Grove TL, Namur O, Holtz F (2018) Crystallization of the lunar magma ocean and the primordial mantle-crust differentiation of the Moon. *Geochim Cosmochim Acta* 234:50–69. <https://doi.org/10.1016/j.gca.2018.05.006>
- Circone S, Agee CB (1996) Compressibility of molten high-Ti mare glass: Evidence for crystal-liquid density inversions in the lunar mantle. *Geochim Cosmochim Acta* 60(14):2709–2720. [https://doi.org/10.1016/0016-7037\(96\)00117-2](https://doi.org/10.1016/0016-7037(96)00117-2)
- Ćuk M, Stewart ST (2012) Making the Moon from a fast-spinning Earth: A giant impact followed by resonant despinning. *Science* 338(6110):1047–1052. <https://doi.org/10.1126/science.1225542>
- Delano JW (1990) Buoyancy-driven melt segregation in the Earth's Moon. I-Numerical results. In: 10th lunar and planetary science conference, pp 3–12
- Dygert N, Hirth G, Liang Y (2016) A flow law for ilmenite in dissolution creep: Implications for lunar cumulate mantle overturn. *Geophys Res Lett* 43(2):532–540. <https://doi.org/10.1002/2015GL066546>
- Dygert N, Lin J-F, Marshall EW, Kono Y, Gardner JE (2017) A low viscosity lunar magma ocean forms a stratified anorthitic flotation crust with mafic poor and rich units. *Geophys Res Lett* 44(22):11,282–211,291. <https://doi.org/10.1002/2017GL075703>

- Elardo SM, Astudillo Manosalva DF (2023) Complexity and ambiguity in the relationships between major lunar crustal lithologies and meteoritic clasts inferred from major and trace element modeling. *Geochim Cosmochim Acta* 354:13–26. <https://doi.org/10.1016/j.gca.2023.05.020>
- Elardo SM, Draper DS, Shearer CK (2011) Lunar Magma Ocean crystallization revisited: bulk composition, early cumulate mineralogy, and the source regions of the highlands Mg-suite. *Geochim Cosmochim Acta* 75(11):3024–3045. <https://doi.org/10.1016/j.gca.2011.02.033>
- Elkins Tanton LT, Van Orman JA, Hager BH, Grove TL (2002) Re-examination of the lunar magma ocean cumulate overturn hypothesis: melting or mixing is required. *Earth Planet Sci Lett* 196(3):239–249. [https://doi.org/10.1016/S0012-821X\(01\)00613-6](https://doi.org/10.1016/S0012-821X(01)00613-6)
- Elkins-Tanton LT, Burgess S, Yin Q-Z (2011) The lunar magma ocean: reconciling the solidification process with lunar petrology and geochronology. *Earth Planet Sci Lett* 304(3):326–336. <https://doi.org/10.1016/j.epsl.2011.02.004>
- Garcia RF, Gagnepain-Beyneix J, Chevrot S, Lognonné P (2011) Very preliminary reference Moon model. *Phys Earth Planet Inter* 188(1):96–113. <https://doi.org/10.1016/j.pepi.2011.06.015>
- Garcia RF, Khan A, Drilleau M, Margerin L, Kawamura T, Sun D, Wieczorek MA, Rivoldini A, Nunn C, Weber RC, Marusiak AG, Lognonné P, Nakamura Y, Zhu P (2019) Lunar seismology: An update on interior structure models. *Space Sci Rev* 215(8):50. <https://doi.org/10.1007/s11214-019-0613-y>
- Ghiorso MS, Sack RO (1995) Chemical mass transfer in magmatic processes IV. A revised and internally consistent thermodynamic model for the interpolation and extrapolation of liquid-solid equilibria in magmatic systems at elevated temperatures and pressures. *Contrib Mineral Petrol* 119(2):197–212. <https://doi.org/10.1007/BF00307281>
- Ghiorso MS, Hirschmann MM, Reiners PW, Kress Iii VC (2002) The pMELTS: a revision of MELTS for improved calculation of phase relations and major element partitioning related to partial melting of the mantle to 3 GPa. *Geochem Geophys Geosyst* 3(5):1–35. <https://doi.org/10.1029/2001GC000217>
- Grove TL, Krawczynski MJ (2009) Lunar mare volcanism: Where did the magmas come from? *Elements* 5(1):29–34. <https://doi.org/10.2113/gselements.5.1.29>
- Harada Y, Goossens S, Matsumoto K, Yan J, Ping J, Noda H, Haruyama J (2014) Strong tidal heating in an ultralow-viscosity zone at the core–mantle boundary of the Moon. *Nat Geosci* 7(8):569–572. <https://doi.org/10.1038/ngeo2211>
- Hartmann WK, Davis DR (1975) Satellite-sized planetesimals and lunar origin. *Icarus* 24(4):504–515. [https://doi.org/10.1016/0019-1035\(75\)90070-6](https://doi.org/10.1016/0019-1035(75)90070-6)
- Hess PC, Parmentier EM (1995) A model for the thermal and chemical evolution of the Moon's interior: Implications for the onset of mare volcanism. *Earth Planet Sci Lett* 134(3):501–514. [https://doi.org/10.1016/0012-821X\(95\)00138-3](https://doi.org/10.1016/0012-821X(95)00138-3)
- Hess PC, Parmentier EM (2001) Thermal evolution of a thicker KREEP liquid layer. *J Geophys Res Planets* 106(E11):28023–28032. <https://doi.org/10.1029/2000JE001416>
- Hood LL, Herbert F, Sonett CP (1982) Further efforts to limit lunar internal temperatures from electrical conductivity determinations. *J Geophys Res Solid Earth* 87(S01):A109–A116. <https://doi.org/10.1029/JB087iS01p0A109>
- Jacobs MHG, van den Berg AP, Schmid-Fetzer R, de Vries J, van Westrenen W, Zhao Y (2022) Thermodynamic properties of geikielite ($MgTiO_3$) and ilmenite ($FeTiO_3$) derived from vibrational methods combined with Raman and infrared spectroscopic data. *Phys Chem Miner* 49(7):23. <https://doi.org/10.1007/s00269-022-01195-5>
- Jing J-J, Lin Y, Knibbe JS, van Westrenen W (2022) Garnet stability in the deep lunar mantle: constraints on the physics and chemistry of the interior of the Moon. *Earth Planet Sci Lett* 584:117491. <https://doi.org/10.1016/j.epsl.2022.117491>
- Johnson TE, Morrissey LJ, Nemchin AA, Gardiner NJ, Snape JF (2021) The phases of the Moon: Modelling crystallisation of the lunar magma ocean through equilibrium thermodynamics. *Earth Planet Sci Lett* 556:116721. <https://doi.org/10.1016/j.epsl.2020.116721>
- Ju DY, Pang RL, Li R, Du W (2022) The initial lunar mantle structure constrained by thermodynamic simulation. *Acta Petrol Sinica* 38(4):1025–1042. <https://doi.org/10.18654/1000-0569/2022.04.05>
- Karato S-i (2013) Geophysical constraints on the water content of the lunar mantle and its implications for the origin of the Moon. *Earth Planet Sci Lett* 384:144–153. <https://doi.org/10.1016/j.epsl.2013.10.001>
- Khan A, Mosegaard K, Williams JG, Lognonné P (2004) Does the Moon possess a molten core? Probing the deep lunar interior using results from LLR and Lunar Prospector. *J Geophys Res Planets*. <https://doi.org/10.1029/2004JE002294>
- Khan A, Connolly JAD, Pommier A, Noir J (2014) Geophysical evidence for melt in the deep lunar interior and implications for lunar evolution. *J Geophys Res Planets* 119(10):2197–2221. <https://doi.org/10.1002/2014JE004661>
- Klaver M, Luu T-H, Lewis J, Jansen MN, Anand M, Schwiebers J, Elliott T (2021) The Ca isotope composition of mare basalts as a probe into the heterogeneous lunar mantle. *Earth Planet Sci Lett* 570:117079. <https://doi.org/10.1016/j.epsl.2021.117079>
- Klaver M, Klemme S, Liu X-N, Hin RC, Coath CD, Anand M, Liszenberg CJ, Berndt J, Elliott T (2024) Titanium-rich basaltic melts on the Moon modulated by reactive flow processes. *Nat Geosci* 17(2):118–123. <https://doi.org/10.1038/s41561-023-01362-5>
- Li H, Zhang N, Liang Y, Wu B, Dygert NJ, Huang J, Parmentier EM (2019) Lunar cumulate mantle overturn: a model constrained by ilmenite rheology. *J Geophys Res Planets* 124(5):1357–1378. <https://doi.org/10.1029/2018JE005905>
- Lin Y, Tronche EJ, Steenstra ES, van Westrenen W (2017) Experimental constraints on the solidification of a nominally dry lunar magma ocean. *Earth Planet Sci Lett* 471:104–116. <https://doi.org/10.1016/j.epsl.2017.04.045>
- Lin Y, Hui H, Xia X, Shang S, van Westrenen W (2020) Experimental constraints on the solidification of a hydrous lunar magma ocean. *Meteorit Planet Sci* 55(1):207–230. <https://doi.org/10.1111/maps.13425>
- Longhi J (1992) Experimental petrology and petrogenesis of mare volcancics. *Geochim Cosmochim Acta* 56(6):2235–2251. [https://doi.org/10.1016/0016-7037\(92\)90186-M](https://doi.org/10.1016/0016-7037(92)90186-M)
- Luo B, Wang Z, Song J, Qian Y, He Q, Li Y, Head JW, Moynier F, Xiao L, Becker H, Huang B, Ruan B, Hu Y, Pan F, Xu C, Liu W, Zong K, Zhao J, Zhang W, Hu Z, She Z, Wu X, Zhang H (2023) The magmatic architecture and evolution of the Chang'e-5 lunar basalts. *Nat Geosci* 16(4):301–308. <https://doi.org/10.1038/s41561-023-01146-x>
- Matsumoto K, Yamada R, Kikuchi F, Kamata S, Ishihara Y, Iwata T, Hanada H, Sasaki S (2015) Internal structure of the Moon inferred from Apollo seismic data and selenodetic data from GRAIL and LLR. *Geophys Res Lett* 42(18):7351–7358. <https://doi.org/10.1002/2015GL065335>
- Maurice M, Tosi N, Samuel H, Plesa A-C, Hüttig C, Breuer D (2017) Onset of solid-state mantle convection and mixing during magma ocean solidification. *J Geophys Res Planets* 122(3):577–598. <https://doi.org/10.1002/2016JE005250>
- Miller GH, Stolper EM, Ahrens TJ (1991) The equation of state of a molten komatiite: 2. Application to komatiite petrogenesis and the Hadean Mantle. *J Geophys Res Solid Earth* 96(B7):11849–11864. <https://doi.org/10.1029/91JB01203>

- Nakamura Y (2005) Farside deep moonquakes and deep interior of the Moon. *J Geophys Res Planets*. <https://doi.org/10.1029/2004JE002332>
- Neal CR, Taylor LA (1989) Metasomatic products of the lunar magma ocean: The role of KREEP dissemination. *Geochim Cosmochim Acta* 53(2):529–541. [https://doi.org/10.1016/0016-7037\(89\)90403-1](https://doi.org/10.1016/0016-7037(89)90403-1)
- Parmentier EM, Zhong S, Zuber MT (2002) Gravitational differentiation due to initial chemical stratification: Origin of lunar asymmetry by the creep of dense KREEP? *Earth Planet Sci Lett* 201(3):473–480. [https://doi.org/10.1016/S0012-821X\(02\)00726-4](https://doi.org/10.1016/S0012-821X(02)00726-4)
- Pommier A, Walter MJ, Hao M, Yang J, Hrubík R (2024) Acoustic and electrical properties of Fe–Ti oxides with application to the deep lunar mantle. *Earth Planet Sci Lett* 628:118570. <https://doi.org/10.1016/j.epsl.2024.118570>
- Prissel TC, Gross J (2020) On the petrogenesis of lunar troctolites: New insights into cumulate mantle overturn and mantle exposures in impact basins. *Earth Planet Sci Lett* 551:116531. <https://doi.org/10.1016/j.epsl.2020.116531>
- Rapp JF, Draper DS (2018) Fractional crystallization of the lunar magma ocean: updating the dominant paradigm. *Meteorit Planet Sci* 53(7):1432–1455. <https://doi.org/10.1111/maps.13086>
- Schmidt MW, Kraettli G (2022) Experimental crystallization of the lunar magma ocean, initial selenotherm and density stratification, and implications for crust formation, overturn and the bulk silicate moon composition. *J Geophys Res Planets* 127(5):e2022JE007187. <https://doi.org/10.1029/2022JE007187>
- Shearer CK, Elardo SM, Petro NE, Borg LE, McCubbin FM (2015) Origin of the lunar highlands Mg-suite: An integrated petrology, geochemistry, chronology, and remote sensing perspective. *Am Miner* 100(1):294–325. <https://doi.org/10.2138/am-2015-4817>
- Snyder GA, Taylor LA, Neal CR (1992) A chemical model for generating the sources of mare basalts: combined equilibrium and fractional crystallization of the lunar magmasphere. *Geochim Cosmochim Acta* 56(10):3809–3823. [https://doi.org/10.1016/0016-7037\(92\)90172-F](https://doi.org/10.1016/0016-7037(92)90172-F)
- Spera FJ (1992) Lunar magma transport phenomena. *Geochim Cosmochim Acta* 56(6):2253–2265. [https://doi.org/10.1016/0016-7037\(92\)90187-N](https://doi.org/10.1016/0016-7037(92)90187-N)
- Thacker C, Liang Y, Peng Q, Hess P (2009) The stability and major element partitioning of ilmenite and armalcolite during lunar cumulate mantle overturn. *Geochim Cosmochim Acta* 73(3):820–836. <https://doi.org/10.1016/j.gca.2008.10.038>
- van Kan PM, Sanloup C, Sator N, Guillot B, Tronche EJ, Perrillat J-P, Mezouar M, Rai N, van Westrenen W (2012) Neutral buoyancy of titanium-rich melts in the deep lunar interior. *Nat Geosci* 5(3):186–189. <https://doi.org/10.1038/ngeo1402>
- Van Orman JA, Grove TL (2000) Origin of lunar high-titanium ultramafic glasses: constraints from phase relations and dissolution kinetics of clinopyroxene-ilmenite cumulates. *Meteorit Planet Sci* 35(4):783–794. <https://doi.org/10.1111/j.1945-5100.2000.tb01462.x>
- Warren PH (1989) KREEP: major-element diversity, trace-element uniformity (almost). In: *Workshop on the moon in transition: Apollo 14 KREEP and evolved lunar rocks*, pp 149–153
- Weber RC, Lin PY, Garnero EJ, Williams Q, Lognonné P (2011) Seismic detection of the lunar core. *Science* 331(6015):309–312. <https://doi.org/10.1126/science.1199375>
- Xu M, Jing Z, Van Orman JA, Yu T, Wang Y (2022) Experimental evidence supporting an overturned iron-titanium-rich melt layer in the deep lunar interior. *Geophys Res Lett* 49(13):e2022GL099066. <https://doi.org/10.1029/2022GL099066>
- Zhang N, Dygert N, Liang Y, Parmentier EM (2017) The effect of ilmenite viscosity on the dynamics and evolution of an overturned lunar cumulate mantle. *Geophys Res Lett* 44(13):6543–6552. <https://doi.org/10.1002/2017GL073702>
- Zhang B, Ge J, Xiong Z, Zhai S (2019) Effect of water on the thermal properties of olivine with implications for lunar internal temperature. *J Geophys Res Planets* 124(12):3469–3481. <https://doi.org/10.1029/2019JE006194>
- Zhang N, Ding M, Zhu M-H, Li H, Li H, Yue Z (2022) Lunar compositional asymmetry explained by mantle overturn following the South Pole-Aitken impact. *Nat Geosci* 15(1):37–41. <https://doi.org/10.1038/s41561-021-00872-4>
- Zhao Y, de Vries J, van den Berg AP, Jacobs MHG, van Westrenen W (2019) The participation of ilmenite-bearing cumulates in lunar mantle overturn. *Earth Planet Sci Lett* 511:1–11. <https://doi.org/10.1016/j.epsl.2019.01.022>
- Zhong S, Parmentier EM, Zuber MT (2000) A dynamic origin for the global asymmetry of lunar mare basalts. *Earth Planet Sci Lett* 177(3):131–140. [https://doi.org/10.1016/S0012-821X\(00\)00041-8](https://doi.org/10.1016/S0012-821X(00)00041-8)

Springer Nature or its licensor (e.g. a society or other partner) holds exclusive rights to this article under a publishing agreement with the author(s) or other rightsholder(s); author self-archiving of the accepted manuscript version of this article is solely governed by the terms of such publishing agreement and applicable law.